-RESEARCH PAPER-

International Journal of Mining and Geo-Engineering

IJMGE

IJMGE 58-3 (2024) 281-287

DOI: 10.22059/IJMGE.2024.368712.595126

Numerical modelling of cohesive-frictional soil behind inclined retaining wall under passive translation mode

Hassan Sarfaraz [a], Mohammad Hossein Khosravi [b, *], Thirapong Pipatpongsa [c]

[a] *School of Mining Engineering, College of Engineering, University of Tehran, Tehran, Iran.*

[b] *Department of Mining Engineering, Faculty of Engineering, University of Birjand, Birjand, Iran.*

[c] *Department of Civil Engineering, National Yang Ming Chiao Tung University, Hsinchu, Taiwan.*

Article History:

Received: 26 November 2023.

Revised: 03 February 2023.

Accepted: 07 May 2024.

ABSTRACT

Accurate assessment of horizontal earth pressure acting upon retaining walls is crucial for the effective and secure design of these constructions. Not only active earth pressure but also the arching phenomenon plays a significant role in passive earth pressure distribution. In this study, using the finite difference method (FDM), some numerical models are simulated to examine the influence of soil strength properties and wall inclination on the earth pressure and ground deformation. The development of shear bands as well as the trajectories of principal stress inside the backfill are investigated. The results of this study show that the failure surface behind the retaining wall under passive mode is generally nonlinear and will become linear only if the wall surface is frictionless. Among the existing theories, the stress distribution provided by the classical theory of Coulomb (1776) shows a better agreement with the numerical data compared to arching-based theories and the classical theory of Rankine (1857). Considering the root mean square error (RMSE) falling within the approximate range of 0.2 to 0.5, it can be inferred that the numerical modelling results demonstrate acceptable agreement with the Coulomb theory. These findings are consistent with the experimental results of Fang et al. (2002).

Keywords: *Cohesive-frictional soil; Inclined retaining wall; Passive earth pressure; Numerical modeling.*

1. Introduction

The successful design and construction of retaining walls heavily rely on accurately estimating horizontal earth pressure. This pivotal factor not only influences structural stability but also affects the choice of construction materials and techniques. The precise estimation of horizontal earth pressure is essential for ensuring the structural integrity of the retaining wall, thereby playing a crucial role in preventing undesirable movements and potential failures. Methodical evaluation and estimation of horizontal earth pressure empower engineers to make informed decisions, enhancing the overall performance and longevity of retaining wall systems.

Theoretical investigations of the earth pressure exerted on a rigid retaining wall were carried out by Coulomb [1] and Rankine [2]. The estimation of lateral earth pressure applied to the structure plays a crucial role in the design of retaining structures. These classical theories assumed a triangular distribution of the passive pressures with maximum pressure acting on the wall toe. However, various experimental studies [3-9] and numerical models [10-16] showed that the pressure distribution behind retaining structures with rough faces is characterized by a curvilinear pattern. The concept of soil arching, first introduced by Terzaghi [17], has been employed by various scholars to predict the passive earth pressure acting behind the retaining wall [18, 19].

Pain et al. [20] presented a formulation for seismic passive earth pressure in non-cohesive soil for translation wall movement, employing the pseudo-static method. When considering static conditions and a vertical wall, their equation exhibits high sensitivity to the wall height. It was observed that the normal earth pressure at the upper portion of the wall becomes negative for wall heights exceeding 1 meter. However, it is expected that the passive earth pressure should be positive along the entire length of the wall. This limitation in the developed formulation is apparent. Alqarawi et al. [21] proposed a formulation to compute the passive earth pressure of granular sloping backfill on a rigid retaining structure by extension of Terzaghi's [17] log-spiral method. Lu et al. [14] conducted numerical investigations to study the three-dimensional distribution of passive earth pressure under three displacement modes. Zhang et al. [22] developed an approach based on the elastic theory to compute the earth pressure acting on rigid retaining structures for three displacement movements.

Limited research has been conducted on estimating the earth pressure distribution in cohesive backfill. Cai et al. [23] proposed a method to calculate the passive earth pressure in cohesive soil, specifically focusing on vertical retaining walls. The researchers assumed a symmetric curve for the major principal stress trajectory within the failure wedge, which was similar to Handy's [24] assumption. However, other researchers [18, 19, and 25] have pointed out that the major principal stress path in the failure zone exhibits an asymmetric geometry.

It is worth noting that in a fully rough wall, their approach does not yield reasonable results, and the failure surface orients along the wall, indicating a drawback in their theory. Furthermore, their approach predicts an unusually high-pressure value at the wall base, which is another limitation of their solution. Ghaffari and Shahir [25] developed

* Corresponding author. *E-mail address:* mh.khosravi@birjand.ac.ir (M. H. Khosravi).

a theoretical method to estimate the passive earth pressure of cohesive soil; however, they did not consider the wall batter in their research.

In order to comprehensively address these limitations, several numerical models, based on the FDM method, are conducted. These models aim to offer predictive insights into the behavior of passive earth pressure within cohesive soil structures, particularly focusing on walls featuring a diverse range of batter inclinations. The outcomes obtained from these numerical investigations are meticulously presented, and thoroughly discussed, and are aimed at offering critical insights into the behavior of passive earth pressure in practical retaining wall design.

2. Numerical modelling

2.1. Model configuration

In this section, using Flac2D software as a finite difference method [26], some numerical models are carried out. The objective is to investigate the failure surface at various angles of interface friction angle and wall batter. The lateral boundaries were fixed in the horizontal direction; the bottom boundary remains fixed both horizontally and vertically. The geometry is displayed in Figure 1. The sensitivity analysis of mesh size shows that a smaller size of 10 cm does not significantly affect the outcomes. Consequently, this mesh dimension was selected, resulting in a grid configuration of 150×44 for this study. The wall height is 4 m, and the model length is 15 m. To mitigate the influence of the lower boundary on the findings, the base of the wall was positioned 0.4 meters higher than the soil bottom.

The modelling of the retaining wall involved employing structural beam elements connected to the soil grid. To simulate the interaction between the soil and wall, a contact surface was established. The backfill material was assumed to exhibit elastic-plastic behavior, and the Mohr-Coulomb failure criterion was applied, using the following material parameters: E=24 MPa, ν=0.3, γ=20 kN/m^3, φ=32°, K_n=10 GPa/m, and K_s=0.5 GPa/m.

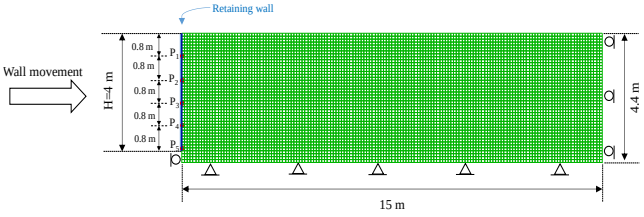

Figure 1. The Geometry of Numerical model.

Prior to any wall movement, the backfill was in a state of static equilibrium, commonly referred to as the at-rest condition. To model the passive mode, a horizontal displacement of 0.2 times the wall height was applied, and subsequent monitoring was conducted to observe the deformation of the backfill.

2.2. The formation of shear bands

The distributions of shear strain increments of granular soil behind the inclined wall are indicated in Figure 2. According to this figure, failure surface and shear bonds appear in the backfill. For δ=0°, the shear line is linear and is initiated in the wall toe. For δ>β, the second shear line emerges. Furthermore, the wedge-shaped failure zone expands with an increase in the soil-wall interface friction angle.

Figure 3 illustrates the variations in shear strain increments within the non-cohesive soil situated behind the vertical wall as the wall experiences displacement, where Δx represents the accumulated wall displacement from its initial position. As depicted in this figure, two shear bands are discernible within the backfill. The initial shear band originates at the wall base and extends upwards into the backfill. The second shear band originates at the upper portion of the wall and extends obliquely downward, intersecting with the first shear band.

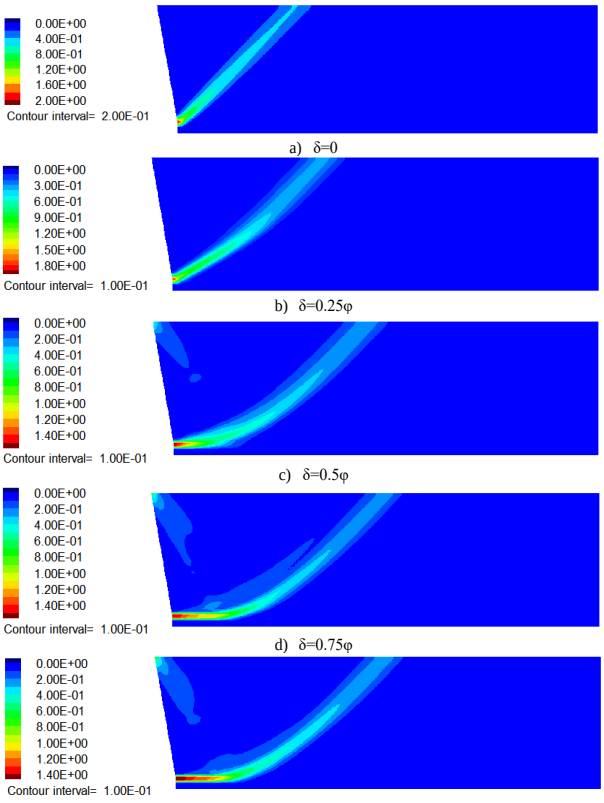

Figure 2. The contours of shear strain increment (γ=20kN/m3, φ=32°, c=0, β=10°).

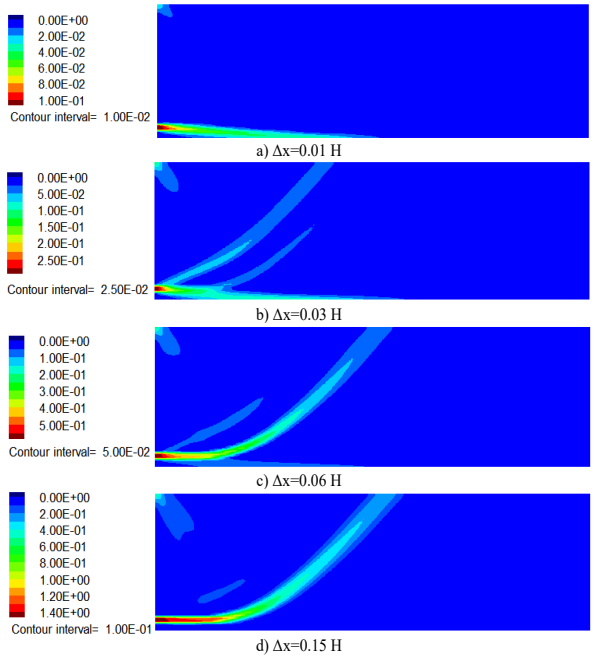

Figure 3. The contours of shear strain increment, where Δx denotes the accumulated wall displacement (γ=20 kN/m3, φ=32°, δ=0.5φ, β=0°).

The geometry of the first shear band is nonlinear, marking a clear departure from Coulomb [1]. The secondary shear band is not adequately addressed by classical theories, although it is taken into account in conventional approaches to the partitioning of the earth wedge.

Figure 4 illustrates the contours that depict the shear strain increment and the plasticity indicator within the backfill under the final steady-state condition. These contours provide insight into the variations observed under different scenarios involving soil properties and wall batters. This graph shows the failed points of soil caused by shearing and tension. In the passive mode, soil failure primarily occurs due to shearing, with these points indicating the locations of slip lines. As illustrated in this figure, an increase in the wall batter angle leads to a reduction in the angle formed between the second shear line and the alignment of the wall.

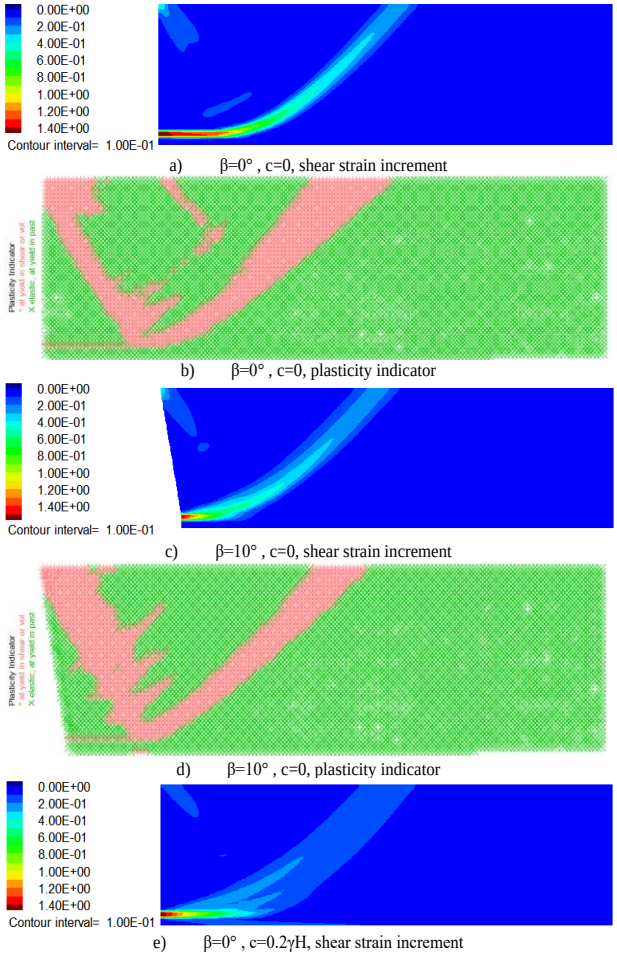

Figure 4. The contours of shear strain increment and plastic indicator (γ=20 kN/m3, φ=32°, δ=0.5φ).

2.3. Earth pressure redistribution

The alterations in the lateral earth pressure occurring as non-cohesive soil moves against the vertical wall are shown in Figure 5. To capture these variations, five specific reference points (labeled as P1 to P5 in Figure 1) are utilized for recording the earth pressure data.

2.4. Principal stress trajectory

The examination of principal stress trajectories has been conducted, as indicated in Figure 6. As observed in this figure, the soil elements adjacent to the wall have a high-stress level, whereas those located at a greater distance from the wall experience comparatively lower stress levels. The major principal stress path of the upper right of the backfill area is approximately horizontal, while the lower-left area of the backfill close to the wall exhibits an inclined major principal stress path, demonstrating a significant influence from the soil arching phenomenon. This trajectory of σ1 aligns with the assumptions made by Cao et al. [19] and Patel and Deb [27]. However, Dalvi and Pise [18] and Pain et al. [20] considered a convex trajectory for major principal stress.

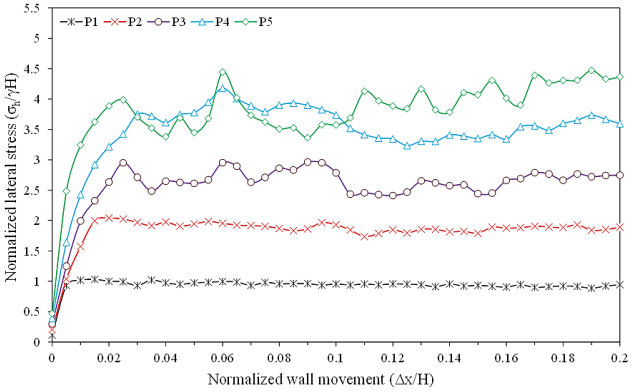

Figure 5. Changes in horizontal earth pressure by wall movement (γ=20 kN/m3, φ=32°, δ=0.5φ, c=0, β=0°).

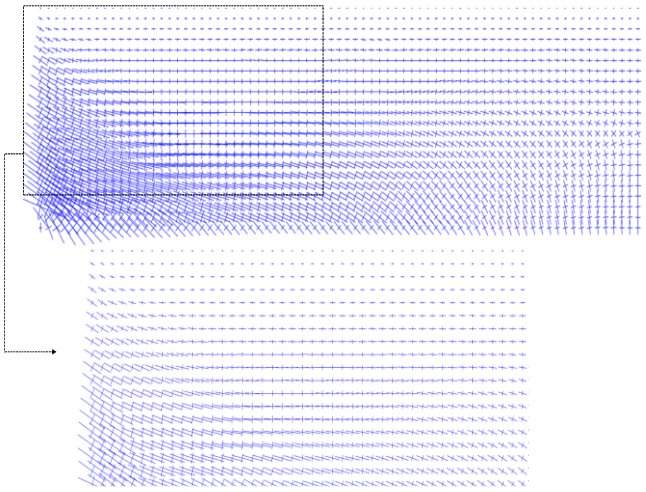

Figure 6. Principal stress vectors (γ=20 kN/m3, φ=32°, δ=0.5φ, β=0°).

3. Stress distribution within the failure wedge

The stress distribution achieved in numerical modelling behind the wall is shown in Figure 5 to Figure 9. The backfill parameters are ϕ=32°, H=4m, γ=20kN/m3, c=16kPa, β=10°, and three values for δ (δ=0, δ=0.5ϕ, and δ=0.75ϕ). Based on Figure 7 to Figure 9, it becomes evident that vertical and shear stresses increased to their maximum amount at the wall toe. Furthermore, the failure wedge zone expands with an increase in the wall-soil interface friction angle.

4. The comparison of the numerical data with the analytical methods

In this section, the numerical modelling results are compared with pre-existing related theories. It is worth mentioning that the Coulomb [1] method is used for granular soil in scenarios involving both vertical and inclined retaining walls.

4.1. Granular backfill behind vertical walls

Figure 10 illustrates the lateral earth pressure distribution acting upon a vertical wall in the context of cohesionless soil. The data presented in this graph were derived based on specific backfill characteristics, including γ=20 kN/m^3, φ=32° and δ=16°, and β=0°. The Coulomb [1] theory includes interface friction angle in the coefficient of later earth pressure, while Rankine [2] does not consider this parameter. This figure shows that the arching phenomenon occurred in the lower zone

of the wall. Additionally, numerical data have an acceptable agreement with the Coulomb [1] theory. However, the method of Cai et al. [23] tends to overestimate the horizontal passive earth pressures exerted against the retaining wall.

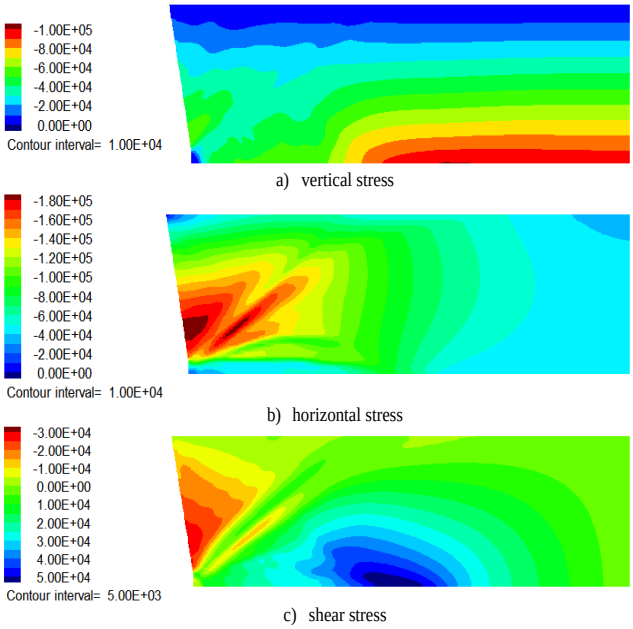

Figure 7. Stress distribution in the proposed method and numerical modelling for δ=0°.

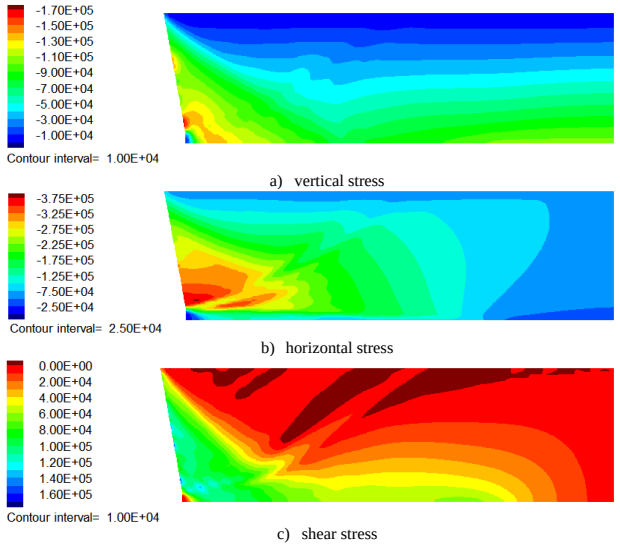

Figure 8. Stress distribution in the proposed method and numerical modelling for δ=0.5ϕ.

4.2. Cohesive backfill behind vertical walls

Figure 11 illustrates how soil cohesion affects the distribution of horizontal earth pressure behind the wall. The soil characteristics considered in this analysis include γ=20 kN/m^3, φ=32°, δ=16°, and β=0°, where the soil cohesion varied from 0.1γH to 0.2γH. The theoretical prediction of lateral passive earth pressure developed by Cai et al. [23] and Ghaffari and Shahir [25] are also presented in this figure. Note that these theories are limited to vertical retaining walls. The theory established by Cai et al. [23] predicts very large lateral passive earth pressures at the lower section of the wall, which seems unrealistic. This drawback of Cai et al. [23] method is discussed by Ghaffari and Shahir [25].

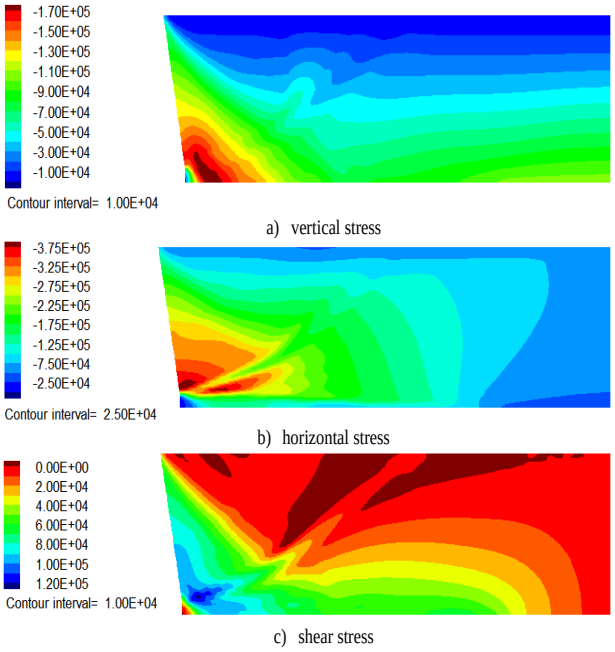

Figure 9. Stress distribution in the proposed method and numerical modelling for δ=0.75ϕ.

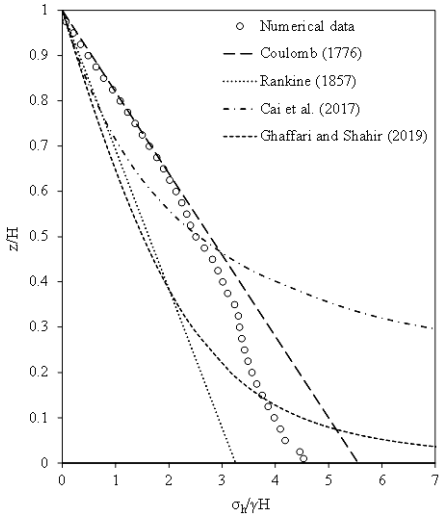

Figure 10. Horizontal earth pressure distribution against a vertical wall for granular soil.

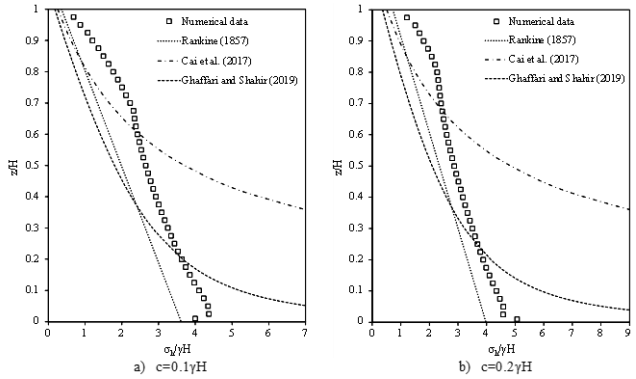

Figure 11. Horizontal earth pressure distributions against a vertical wall for cohesive soil.

4.3. Granular backfill behind inclined walls

Figure 12 illustrates how the inclination of the wall, also known as the wall batter, impacts the distribution of horizontal earth pressure behind the wall. The specific parameters employed for this analysis are γ=20 kN/m³, c=0, φ=32°, and δ=16°. Notably, the wall batter changed from 5° to 10°. According to this figure, the numerical results are in good agreement with the results of Coulomb [1]. Moreover, the utilization of the Rankine [2] theory is put into practice within a virtual context, specifically referring to a vertical surface in alignment with the wall base. The notion of this virtual plane was first introduced by Taylor [28] as an extension of Rankine [2] original theory, particularly applicable to inclined retaining walls. This virtual plane represents a hypothetical surface where shear stresses are negligible.

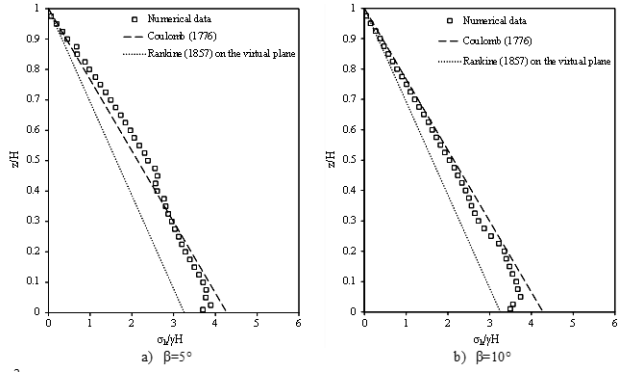

Figure 12. Horizontal earth pressure distributions against battered walls for cohesionless soil.

4.4. Cohesive backfill behind inclined walls

The distributions of horizontal earth pressure of cohesive soil against a wall with various batters are indicated in Figure 13. The calculations for these graphs are based on the following backfill properties: γ=20 kN/m³, φ=32°, and δ=16°. The horizontal earth pressure increases and decreases with an increase in cohesion and wall batter.

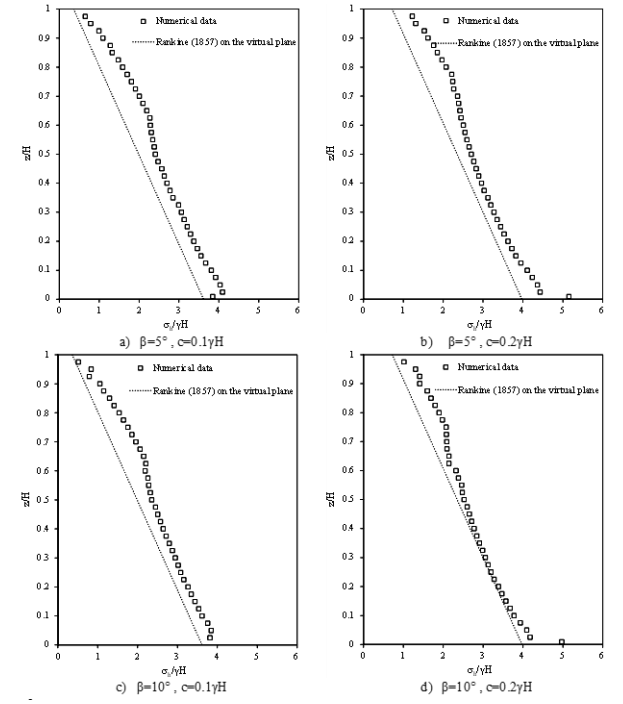

Figure 13. Horizontal earth pressure distributions against battered walls for cohesive soil.

5. Results and discussions

The determination of the thrust lateral force acting on the wall can be accomplished by performing an integration of the horizontal earth pressure concerning the vertical distance.

$$P_h = \int_0^H \sigma_h \, dz \tag{1}$$

The moment of the horizontal pressure around the wall base can be achieved utilizing the following equation.

$$M_h = \int_0^H \sigma_h \, z dz \tag{2}$$

The elevation at which the horizontal thrust force is applied can be determined by dividing Equation (2) by Equation (1).

$$h_p = \frac{M_h}{P_h} \tag{3}$$

The lateral thrust force as well as the point of application of this force for granular soil situated behind inclined walls are shown in Figure 14. Additionally, the theory of Coulomb [1] is also plotted in this figure. The horizontal thrust force values, as indicated in Figure 14(a), are expressed in the form of a normalized ratio denoted as K_{ph}.

$$K_{p_h} = \frac{P_h}{0.5\gamma H^2} \tag{4}$$

According to Figure 14(a), the numerical data closely aligns with the Coulomb [1] theory. Also, Figure 14(b) shows a good agreement between the numerical data and two classical theories, both of which overlap with each other.

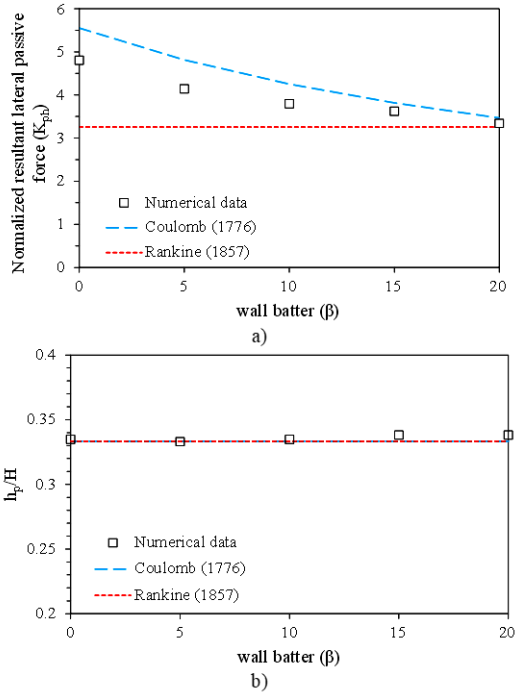

Figure 14.- a) lateral thrust force, b) the application point of lateral thrust.

The variation of K_{ph} with wall movement is shown in Figure 15. In numerical modelling, K_{ph} initially increases as wall movement increases. After reaching a peak value, with further increases in wall movement, this value decreases and eventually stabilizes at a constant level. In addition, the classic theories of Coloumb [1] and Rankine [2] are plotted in this figure. It is noteworthy that the results of these theories remain unchanged regardless of wall movement. As the wall movement approached a condition referred to as "passive wall movement", earth pressures stabilized at consistent magnitudes. In this model, a passive wall movement range of approximately Δx=0.08H was recorded. Fang et

al. [4] concluded that Δx>0.12H, the passive earth thrust reaches a constant value, irrespective of the backfill density.

6. Conclusions

The arching effect plays a significant role in the retaining wall design in the passive earth pressure distribution. In this work, several numerical simulations, based on the finite difference method, were carried out to predict passive earth pressure for cohesive soil behind inclined walls.

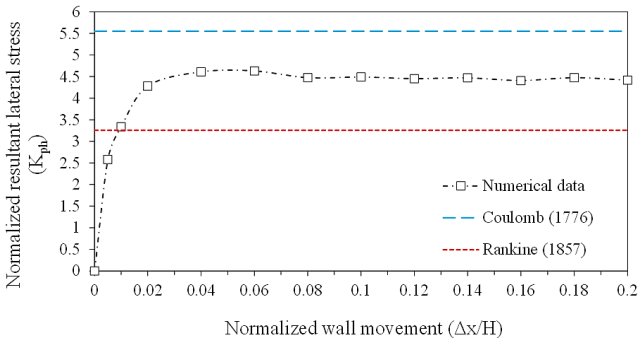

Figure 15. Variation of Kph with wall movement.

Furthermore, shear bands, earth pressure distributions, and principal stress trajectory were analyzed. The results of numerical data were compared with pre-existing analytical approaches. Additionally, the lateral thrust force and application height of thrust were investigated. In summary, the following conclusions can be drawn from this research:

- Contrary to the assumption of creating a linear failure surface behind the retaining wall under the passive mode adopted by many researchers, this failure surface is generally nonlinear and will become linear only if the wall surface is frictionless.
- As the wall moves towards the soil, two shear bands form inside the backfill. The first shear band initiates at the base of the wall and extends nonlinearly upward into the backfill, while the second shear band initiates at the top of the wall and extends obliquely downward to reach the first shear band.
- In theories based on the arching phenomenon, the lateral pressure against the wall tends to infinity at the heel of the wall, which is incorrect.
- Among the classical theories, the stress distribution proposed by the Coulomb [1] theory shows an acceptable agreement with numerical data, while the Rankine [2] theory underestimates the passive earth pressure on the wall. As also mentioned by Fang et al. [4], this is most likely due to the fact that wall friction is neglected in the Rankine's theory. Consequently, the root mean square error (RMSE) between numerical modelling and the Coulomb theory for vertical and battered walls with angles of 5 and 10 degrees is determined to be 0.53, 0.38, and 0.19, respectively.
- For a nearly vertical wall, the resultant lateral passive force is overestimated by the Coulomb [1] theory while underestimated by the Rankine [2] theory. However, as the wall batter increases, the difference decreases and both classical theories provide a good approximation for the lateral passive force on the wall. The thrust application point, predicted by both classical theories, is in good agreement with the numerical data.

Symbol list

z	vertical distance from the surface
σ_h	passive horizontal earth pressure
P_h	resultant horizontal force
M_h	moment of the horizontal stress
h_p	application point of resultant thrust force
γ	unit weight
c	cohesion
φ	internal friction angle
δ	interface friction angle
H	wall height
β	angle of wall batter
E	young modulus
ν	Poisson's ratio
k_n	normal stiffness
k_s	shear stiffness

Declaration

The authors declare that they have no known competing financial interests or personal relationships that could have appeared to influence the work reported in this paper.

REFERENCES

[1] C. A. Coulomb. (1776) Essai sur une application des regles de maximis et minimis a quelques problemes de statique relatifs a l'architecture (essay on maximums and minimums of rules to some static problems relating to architecture).

[2] W. J. M. Rankine. (1857). II. On the stability of loose earth," *Philos. Trans. R. Soc. London*, 147: 9–27.

[3] Y.-S. Fang, T.-J. Chen, and B.-F. Wu. (1994). Passive earth pressures with various wall movements, *J. Geotech. Eng.*, 120 (8): 1307–1323.

[4] Y.-S. Fang, Y.-C. Ho, and T.-J. Chen. (2002). Passive earth pressure with critical state concept, *J. Geotech. Geoenvironmental Eng.*, 128 (8): 651–659.

[5] R. Xu, Y. Chen, Z. Yang, and X. Gong. (2002). Experimental research on the passive earth pressure acting on a rigid wall, *CHINESE J. Geotech. Eng. Ed.*, 24 (5): 569–575.

[6] T. S. O'Neal and D. J. Hagerty. (2011). Earth pressures in confined cohesionless backfill against tall rigid walls—a case history, *Can. Geotech. J.*, 48 (8): 1188–1197.

[7] M. H. Khosravi, T. Pipatpongsa, and J. Takemura. (2013). Experimental analysis of earth pressure against rigid retaining walls under translation mode, *Géotechnique*, 63 (12): 1020–1028.

[8] H. W. Ying, J. H. Zhang, X. G. Wang, B. H. Li, and W. Zhu. (2016). Experimental analysis of passive earth pressure against rigid retaining wall under translation mode for finite soils, *Chinese J. Geotech. Eng.*, 38 (6): 978–986.

[9] X. I. A. Jun-wu, D. O. U. Guo-tao, S. U. Qiong, and others. (2019). An experiment study on the non- limit passive earth pressure of clay under different displacement modes, *J. Southwest Jiaotong Univ.*, 54 (4): 769–777.

[10] S. Liu, Y. Xia, and L. Liang, (2018). A modified logarithmic spiral method for determining passive earth pressure *J. Rock Mech. Geotech. Eng.*, 10 (6): 1171–1182.

[11] F. Chen, Y. Lin, and J. Yang. (2020). Passive earth pressure of narrow cohesionless backfill against inclined rigid retaining walls under translation mode, *Soils Found.*, 60 (5): 1226–1240.

[12] F. Chen, Y. Lin, J. Yang, and M. Huang. (2021). Passive Earth pressure of narrow cohesionless backfill against rigid retaining walls rotating about the base, *Int. J. Geomech.*, 21 (1): 6020036.

[13] W. Kejia, P. Yu, and Y. Liu, "Simulation of Passive Earth Pressure

against Retaining Wall Considering Wall Movement Mode," in *IOP Conference Series: Earth and Environmental Science*, 2021, vol. 714, no. 2.

[14] K. Lu, G. Zhou, and K. Shi. (2021). Numerical study of 3D passive earth pressure on a rigid retaining wall in three displacement modes, *Arab. J. Geosci.*, 14 (19): 1–10.

[15] H. Chen, F. Chen, and Y. Lin. (2022). Slip-Line Solution to Earth Pressure of Narrow Backfill against Retaining Walls on Yielding Foundations, *Int. J. Geomech.*, 22 (5): 4022051.

[16] M. Jiang, M. Niu, and W. Zhang. (2022). DEM analysis of passive failure in structured sand ground behind a retaining wall, *Granul. Matter*, 24 (2): 1–22.

[17] K. Terzaghi. (1943). Theoretical soil mechanics. John Wiley & Sons, New York., *Theor. soil Mech. John Wiley Sons, New York.*

[18] R. S. Dalvi and P. J. Pise. (2012). Analysis of arching in soil-passive state, *Indian Geotech. J.*, 42 (2): 106–112.

[19] W. Cao, T. Liu, and Z. Xu. (2019). Calculation of passive earth pressure using the simplified principal stress trajectory method on rigid retaining walls, *Comput. Geotech.*, 109: 108–116.

[20] A. Pain, Q. Chen, S. Nimbalkar, and Y. Zhou. (2017). Evaluation of seismic passive earth pressure of inclined rigid retaining wall considering soil arching effect, *Soil Dyn. Earthq. Eng.*, 100: 286–295.

[21] A. S. Alqarawi, C. J. Leo, D. S. Liyanapathirana, L. Sigdel, M. Lu, and P. Hu. (2021). A spreadsheet-based technique to calculate the passive soil pressure based on the log-spiral method, *Comput. Geotech.*, 130.

[22] L. Zhang, F. Dang, X. Wang, J. Ding, J. Gao, and Y. Zhang. (2022). Estimation of earth pressure against retaining walls with different limited displacement modes based on elastic theory, *J. Mt. Sci.*, 19 (1): 289–304.

[23] Y. Cai, Q. Chen, Y. Zhou, S. Nimbalkar, and J. Yu. (2017). Estimation of passive earth pressure against rigid retaining wall considering arching effect in cohesive-frictional backfill under translation mode, *Int. J. Geomech.*, 17 (4): 4016093.

[24] R. L. Handy. (1985). The Arch in Soil Arching, *J. Geotech. Eng.*, 111 (3): 302–318.

[25] K. Ghaffari Irdmoosa and H. Shahir. (2019). Analytical solution for passive earth pressure of c-φ soil using principal stress rotation assumption, *J. Geoengin.*, 14 (1): 31–39.

[26] Consulting group Itasca. (2016). *FLAC2D Fast Lagrangian Analysis of Continua in 2 Dimension*.

[27] S. Patel and K. Deb. (2022). Experimental and analytical study of passive earth pressure behind a vertical rigid retaining wall rotating about base, *Eur. J. Environ. Civ. Eng.*, vol. 26 (6): 2371–2399.

[28] D. W. Taylor. (1948). *Fundamentals of soil mechanics*, 66 (2): LWW.